Materials and Design 43 (2013) 307–321

Contents lists available at SciVerse ScienceDirect

Materials and Design

journal homepage: www.elsevier.com/locate/matdes

# High velocity impact response of Kevlar-29/epoxy and 6061-T6 aluminum laminated panels

A.A. Ramadhan, A.R. Abu Talib *, A.S. Mohd Rafie, R. Zahari

*Department of Aerospace Engineering, University Putra Malaysia, 43400 Selangor, Malaysia*

ARTICLE INFO

*Article history:*
Received 20 April 2012
Accepted 18 June 2012
Available online 4 July 2012

*Keywords:*
Composite structure
High velocity
Energy absorption
Impact behavior

ABSTRACT

The high velocity impact response of composite laminated plates has been experimentally investigated using a nitrogen gas gun. Tests were undertaken on sandwich structures based on Kevlar-29 fiber/epoxy resin with different stacking sequence of 6061-T6 Al plates. Impact testing was conducted using cylindrical shape of 7.62 mm diameter steel projectile at a range of velocities (180–400 m/s) were investigated to achieve complete perforation of the target. The numerical parametric study of ballistic impact caused by same conditions in experimental work is undertaken to predict the ballistic limit velocity, energy absorbed by the target and comparison between simulation by using ANSYS Autodyn 3D v.12 software and experimental work and study the effects of shape of the projectile with different (4, 8 and 12 mm) thicknesses on ballistic limit velocity. The sequence of Al plate position (front, middle and back) inside laminate plates of composite specimen was also studied. The Al back stacking sequence plate for overall results obtained was the optimum structure to resist the impact loading.

The results obtained hereby are in good agreement with the experimental (maximum error of 3.64%) data where it has been shown that these novel sandwich structures exhibit excellent energy absorbing characteristics under high velocity impact loading conditions. Hence it is considered suitable for applications of armor system.



## 1. Introduction

Composite materials have applications in a wide range of industrial engineering fields due to their inherently superior mechanical properties such as high strength-to-weight ratio and high stiffness as aircraft industry, civil, mechanical, defense, and other disciplines in which they are subjected to a wide spectrum of loading during in-service use. Polymer matrix composites (PMCs) are attractive because they are lighter, stronger, and stiffer than unreinforced polymers or conventional metals, with the additional advantage that their properties and form can be tailored to meet the needs of a specific application. High-performance fibers such as carbon, boron, graphite, and Kevlar are of the highest interest for military and aerospace composite applications that can be used at high temperatures and resist corrosion better than conventional metals or plastics. PMCs have been widely adopted in military applications to resist foreign object impact loading. During ballistic impact, PMC retards the projectile by absorbing its kinetic energy through different mechanisms such as deformation of the composite, delamination, and shear between layers. The condition for perforation, also called the ballistic limit, is certainly the most important factor for designing a suitable protective structure. It is important to understand the dynamic behavior of composite structures and the associated damage mechanisms in order to effectively use the composite as a protective structure.

Significant research has been carried out on the behavior of composite materials under impact loading. However, works on ballistic impacts, particularly on Kevlar/epoxy composites are still in their infancy. Hazell et al. [1] have experimentally studied the response of a bonded carbon–fiber-reinforced plastic composite panel to impact, penetration, and perforation by a high-velocity steel sphere. Zhu et al. [2] investigated the response of woven Kevlar/polyester laminates of varying thicknesses to quasi-static and dynamic penetration by cylindroconical projectiles. Ballistic limits were also determined and terminal velocities were measured. It was reported that deliberately introduced delamination and changes in the volume fraction did not result in significant changes in the impact resistance. The damage pattern for dynamic loading was, however, quite different from that in the corresponding quasi-static penetration case.

Hou et al. [3] identified and discussed the ballistic performance, quasi-static and impact perforation of metallic sandwich structures with aluminum foam and studied the effects of several key parameters as impact velocity, skin thickness, thickness, density of foam core, and projectile shapes on the ballistic limit and energy absorption of the panels during perforation of impact loading. Cheng et al. [4] developed a model for high-velocity impact on

* Corresponding author. Tel.: +60 3 89466400; fax: +60 3 86567125.
*E-mail address:* ayad_almuhndis@yahoo.com (A.R. Abu Talib).

0261-3069/$ - see front matter © 2012 Elsevier Ltd. All rights reserved.
http://dx.doi.org/10.1016/j.matdes.2012.06.034

**Nomenclature**

| | | | |
|---|---|---|---|
| $\rho$ | density (g/cm$^3$) | $V_r$ | residual velocity (m/s) |
| $v$ | Poisson's ratio | $V_{50}$ | perforation velocity (m/s) |
| $E_1$ | longitudinal Young's modulus (GN/m$^2$) | $E_{Abs}$ | energy absorption by the specimen (J) |
| $E_2$ | transverse Young's modulus (GN/m$^2$) | $m$ | mass of bullet (kg) |
| $V_f$ | volume fraction of fiber (N/m) | $V_b$ | ballistic limit velocity (m/s) |
| $V_i$ | initial velocity (m/s) | $G_m$ | modulus of rigidity of the matrix |

thick composites for predicting the response of thick composite targets. This model was based on a continuum approach, which was built on the framework of an orthotropic constitutive behavior with stress-based failure criteria and a simplified degradation model of the failure of composites. The model was implemented into a hydrodynamic finite element code. Punching, fiber breakage, and delamination were the major energy-absorbing mechanisms of the penetration processes.

Zhao et al. [5] investigated the failure models of T300/epoxy composite laminates at different velocities of 10–300 m/s striking on the laminates $[(45/\text{-}45)_4]_s$, $[(0/45/90/\text{-}45)_2]_s$, and $[(0/45/90/\text{-}45)_4]_s$ and they used a laser velocity device to measure the residual velocities of three types of bullet striking velocities classified as the less, equal, and larger than the ballistic limit velocity by a high-speed gas gun. In the tests, the whole penetration process is recorded by high-speed camera from the front side of targets, and then the fracture and the energy absorption of specimens are analyzed. Under the high velocity impact, the in situ stress distribution is investigated through the reading of strain gages installed on specimens.

An example where the impactor is important is an automobile whereas the examples where the target is important are body armors, bullet proof jackets and fuselage or engine casing in aircrafts. Ravid et al. [6] presented an analysis of ballistic impact behavior of metallic targets using dynamic plasticity approach. For a comprehensive analysis of structures subjected to impact, a detailed understanding of the projectile material and its deformation behavior [6], Specifically, Ravid et al. [6,7] and Ravid and Bodner [8] presented an analytical method for the analysis of deformable metallic targets under high velocity impacts using dynamic plasticity approach. Predicted results were also validated with the experimental observations.

Ravid and Bodner [8] presented a mathematical model for the penetration and perforation of visco-elastic metallic targets impacted with rigid projectiles using dynamic plasticity approach. They analyzed work done by different mechanisms during each stage of penetration and perforation as well as energy absorbed at different stages of penetration and perforation. They considered failure mechanisms like adiabatic shear failure, brittle shear failure and tensile failure in their analysis. Ravid et al. [6,7] refined their previous model to include the two dimensional projectile deformation.

Silva [9] have reported experimental and numerical simulation of ballistic impact on Kevlar-29 impacted with simulated fragments. Numerical modeling was developed and used to obtain an estimate for the limit perforation velocity ($V_{50}$) and simulate failure modes and damage. Good correlation between computational simulation and experimental results was reported, both in terms of deformation and damage of the laminates. Hazell and Thomas [10] presented a high velocity steel sphere with impact energy applied on several hybrid CFRP laminates of different materials and geometries. Kevlar loosely bound to the rear of the CFRP laminate proved to be the most weight-efficient method of dissipating the kinetic energy of the projectile and compared with the impact response of a non-woven symmetrical CFRP laminate with woven laminate over an impact-energy regime of 92–459 J it was found that at lower impact-energies there were strong indications that the non-woven laminate out-performed the woven laminate whereas at the higher impact-energies the ballistic performance was seen to be approximately the same.

Tan and Khoo [11] studied the response of spectra shield laminates to ballistic impacts by projectiles of flat-ended, hemispherical, ogival (CRH 2.5), and conical (300 half-angle) shapes. Ballistic tests showed that flat-ended projectiles cut the laminate through a shearing action whereas hemispherical projectiles perforate the laminates by stretching the spectra filaments to failure resulting in a rectangular hole in the laminates. On the other hand, ogival and conical projectiles perforate the laminates with minimal delamination and tearing of the specimens. The area of the specimens affected by the projectiles appears to increase in size instead of becoming more localized at higher impact velocities. Kumar et al. [12] investigated the ballistic response of laminated composite plates using numerical simulations to determine the ballistic response of thick Kevlar/epoxy composite plates as armor structures. These plates were impacted at velocities between 100 and 1000 m/s, and the authors studied the ballistic impact caused by cylindrical projectiles to obtain an estimate for the ballistic limit velocity, energy absorbed by the plate, and the contact duration. The effect of mass and diameter of the projectile on ballistic limit velocity was also studied. They obtained good results compared with the experimental data presented by other researchers.

Naik and Doshi [13] presented the ballistic impact behavior of typical woven fabric E-glass/epoxy thick composites analytically. Specifically, the energy absorbed by different mechanisms, ballistic limit velocity, and contact duration were determined. Furthermore, the effect of incident impact velocity on contact duration and residual velocity, effect of projectile diameter and mass on ballistic limit velocity, and effect of target thickness on ballistic limit velocity and contact duration were studied. It was reported that shear plugging is the major energy-absorbing mechanism. Kevlar are known to have the highest energy absorbing capability among a variety of composites and therefore is the most widely used material in ballistic applications [2]. Key development criteria for future lightweight military, marine, and aerospace hardware involves the combination of layered and graded structures into multifunctional hybrid systems. Therefore, in order to successfully achieve this, materials that offer an outstanding response to dynamic loading conditions at a lower weight should be selectively arranged to create systems that ensure a high level of protection, for example, against injuries to military personnel from ballistic attacks as well as landmines and other explosions; similarly, against fuselage damage and passenger harm in case of engine failure.

The performance of Alumina armor tiles wrapped with thin layers of several different materials such as carbon–fiber/epoxy, E-glass-/epoxy is achieved by using experimental techniques Nemat-Nasser et al. [14]. Details and results from a two-dimensional finite element model using DYNA2D are presented. The results obtained show that release waves emanating from the projectile

edges reduce the pressure and increase the shear stress at a distance equal to the projectile diameter, ahead of the projectile. The performance of ceramic/composite armor subjected to a projectile impact is analyzed by Grujicic et al. [15]. Alumina ceramic was modeled in Autodyn using a polynomial equation of state, Johnson–Holmquist 2 (JH-2) strength model [16] and JH-2 failure model along with an erosion model. The composite material, S2-glass, is modeled using an orthotropic material model [17].

Silicon carbide square tiles of different areal geometries and manufactured via two different processing routes have been bonded to polycarbonate layers to evaluate their ballistic performance [18]. Four ceramic tile sizes were tested: 85 mm, 60 mm, 50 mm and 33 mm. In each case the residual depth-of-penetration into a polycarbonate semi-infinite backing was recorded. To elucidate the penetration and failure mechanisms, a computational model using the JH-1 ceramic model of the projectile used in the experimental study penetrating into a silicon carbide-faced polycarbonate was implemented in the hydrocode Autodyn-2D that there is a critical dimension of tile that should be used in a silicon carbide-based ceramic-faced mosaic armor system design to ensure optimum system performance when each tile is struck centrally [19]. Ballistic performance of different type of ceramic materials subjected to high velocity impact was investigated in many theoretical, experimental and numerical studies. A comparison of ballistic performance of 95% alumina ceramic and 10% zirconia toughened alumina (ZTA) ceramic tiles was analyzed theoretically and experimentally. Spherical cavity model based on the concepts of mechanics of compressible porous media of Galanov was used to analyze the relation of target resistance and static mechanical properties. Experimental studies were carried out on the ballistic performance of above two types of ceramic tiles based on the depth of penetration (DOP) method, when subjected to normal impact of tungsten long rod projectiles. Typical damaged targets were presented.

Ubeyli et al. [20] studied the ballistic behavior of laminated composite having alumina front and dual phase steel backing layers by using 7.62 mm armor piercing (AP) projectiles under normal impact. The variables used were marten site content of the backing layer and the areal density of the composite. Experimental results showed that utilization of a 6 mm thick alumina front layer which was bonded to dual phase steel enhanced the ballistic resistance of the dual phase steel remarkably.

Preliminary studies have shown that it is possible to manufacture thermoplastic-based composite skin carbon [21] and aluminum foam sandwich structures in a single cold stamping manufacturing operation [22–24]. Reyes [25] investigated the fiber-metal laminates (FMLs) skins and aluminum foam core which were tested under quasi-static and low-velocity impact loading conditions. The low-velocity impact behavior of the sandwich panels was evaluated using an instrumented dropping weight impact tower and modeled using an energy balance approach. The ballistic impact problems on thin composite laminated plates [26,27]. Ballistic impact was imparted with simulated fragments designed in accordance with STANAG-2920 on plates of different thickness. Wijk [28] Slip line field theory is used to obtain the projectile penetration resistance in the target material and energy conservation is used to determine the hole radius in the target.

To the author's knowledge, there is no literature available to investigate the high velocity impact response of fiber Kevlar-29/epoxy with 6061-T6 Al plates using cylindrical, spherical and nose ended 8 mm 4340 steel projectiles. In this paper, effects of projectile velocity, thickness of plates and the sequence of Al plate inside the laminate plates on the ballistic impact behavior of the targets are investigated experimentally and numerically through simulation. The simulations are carried out using ANSYS Autodyn 3D-v.12 software. The novel sandwich plate fabricated in this work can be used in contribution to many applications like vehicles, body armor, aerospace and military applications.

## 2. Experimental methodology

### 2.1. Materials used, properties and fabricating the specimens

The materials used in this work are includes woven fiber Kevlar-29, epoxy resin/hardener type 506/HY 956 and aluminum (Al) plate type 6061-T6 with 0.7 mm thickness. The mechanical properties of these materials have been specified in Table 1.

The volume fraction of fiber $V_f$ (fiber volume/total volume) in composites is very often significantly less than 100%, and it was tested by Weinberg and Schwartz [29] as shown in Table 2, so the volume fraction was selected as 55% in this work, as it was the optimum value compared with other volume fractions for fabricating the specimens.

Three thicknesses (4, 8 and 12 mm) of specimens were fabricated as three types of upper, middle and lower layers in the stacking sequence of Al 6061-T6 plate inside the laminate plate. Hand lay-up method has been used to fabricate all the specimens. Woven roving Kevlar-29 fiber is wound manually in the open mold of glass, which was coated with wax to easily remove the specimen later. Epoxy resin was brushed over and into the woven roving Kevlar-29 fiber with different stacking sequences of Al plate in this way for Kevlar-29 epoxy during the fabrication process as shown in Fig. 1. The time of solidification is about 72 h to provide optimum blend.

Kevlar-29/epoxy with 6061-T6 Al laminated plates with 4, 8 and 12 mm thickness were cut out of square plate 100 × 100 mm by cutting tools to prepare it for impact testing, tensile test, and compression test to obtain the basic mechanical properties as shown in Fig. 2 and the stress strain curve was obtained as shown

**Table 1**
Mechanical properties of fiber Kevlar-29.

| Properties | Material | | |
|---|---|---|---|
| | Kevlar-29 fiber | Aluminum (6061-T6) | Epoxy resin |
| Density (g/cm$^3$) | 1.4 | 2.7 | 1.12 |
| Ultimate tensile strength (MPa) | | 310 | |
| Tensile yield strength (MPa) | 2758 | 276 | 4.84 |
| Modulus of elasticity (GPa) | 62 | 68.9 | 42 |
| Poisson's ratio | | 0.33 | |
| Fatigue strength (MPa) | | 96.5 | |
| Shear strength (MPa) | | 207 | |

**Table 2**
Effect of Vf Kevlar-29/epoxy on strength, modulus and strain [19].

| $V_f$ (%) | Tensile strength (MPa) | Modulus (GPa) | Strain (%) | $V_f$ (%) | Tensile strength (MPa) | Modulus (GPa) | Strain (%) |
|---|---|---|---|---|---|---|---|
| 9 | 2412 | 70.9 | 3.0 | 55 | 2908 | 92.3 | 2.9 |
| 22 | 2915 | 88.5 | 3.0 | 56 | 2921 | 91.0 | 3.0 |
| 28 | 2901 | 92.1 | 2.9 | 57 | 3045 | 91.6 | 3.1 |
| 30 | 3039 | 91.5 | 3.1 | 59 | 2853 | 93.4 | 2.9 |
| 31 | 2908 | 88.9 | 3.0 | 61 | 2756 | 92.0 | 2.8 |
| 34 | 2880 | 89.8 | 3.0 | 63 | 2749 | 91.7 | 2.8 |
| 43 | 3114 | 91.3 | 3.1 | 64 | 2536 | 90.8 | 2.6 |
| 44 | 2928 | 92.4 | 3.0 | 65 | 2894 | 91.3 | 3.0 |
| 45 | 2908 | 91.1 | 2.9 | 68 | 2673 | 90.5 | 2.7 |
| 46 | 3016 | 92.4 | 3.0 | 70 | 2418 | 94.0 | 2.5 |
| 50 | 2887 | 93.1 | 2.9 | 72 | 2219 | 90.8 | 2.3 |
| 51 | 3039 | 92.8 | 3.0 | 76 | 2081 | 90.0 | 2.2 |
| 55 | 2942 | 93.6 | 2.9 | 100 | 2184 | 91.0 | 2.3 |

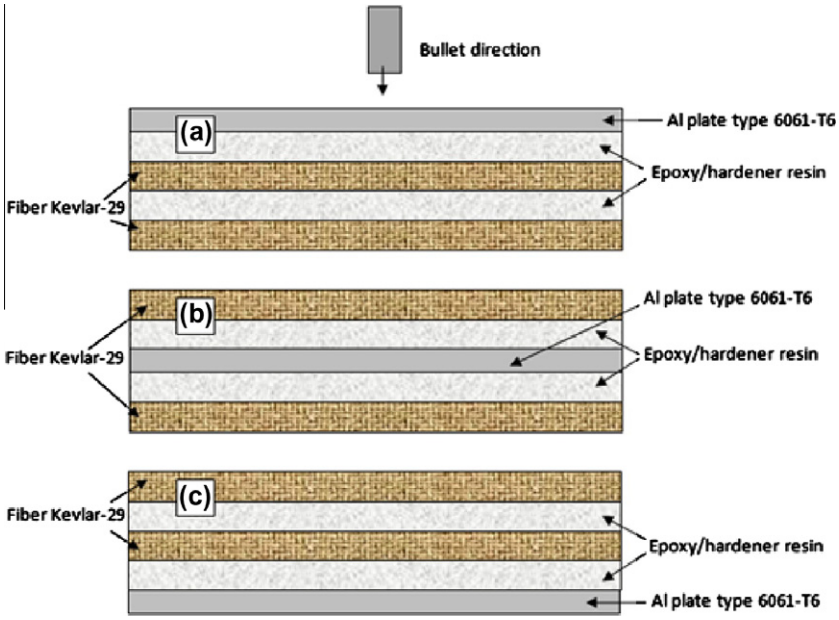


**Fig. 1.** Stacking sequence of Al 6061-T6 plate inside the laminated plate relative to bullet impact; (a) upper Al plate, (b) middle Al plat and (c) lower Al plate.

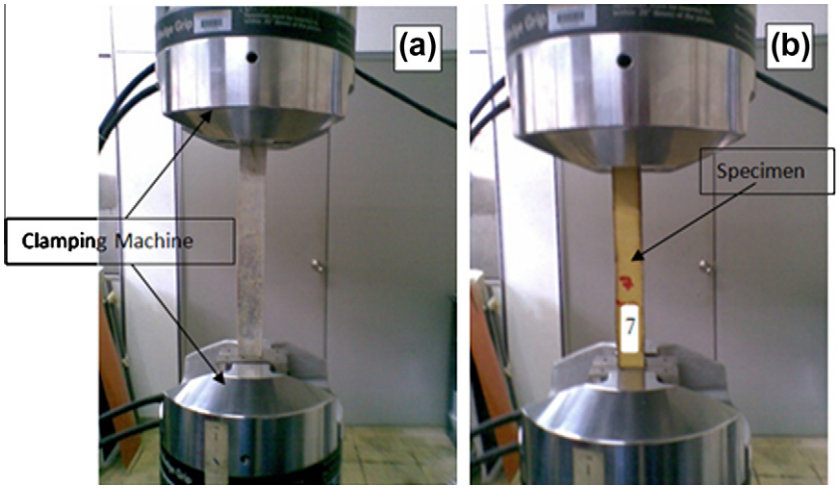


**Fig. 2.** Specimens under test (a) tensile test and (b) compression test.

in Fig. 3 for tensile and compression tests for different stacking sequences of Al plate, but the main objective in this work was the fabrication of a novel sandwich structure and its subsequent test by high impact loading.

The total specimens tested in this work were 42 laminated plates; 12 for compression and tensile tests and 30 for high velocity impact tests which were subjected to cylindrical bullets with different initial velocity impact as shown in Table 3.

### 2.2. Gas gun and bullet selection

The instrumented impact test equipment used in this study was a gas gun impact tester as used by Sultan [30] as shown in Fig. 4. The general features of the testing apparatus designed in order to launch the projectiles are shown in Fig. 5. The main components of the gas gun are the 2200 Psi pressure tank, the purpose-built ring section for compressed gas, the 4 m long smooth barrel and (60, 60 and 40 cm) dimensions of box chamber to hold the specimen inside

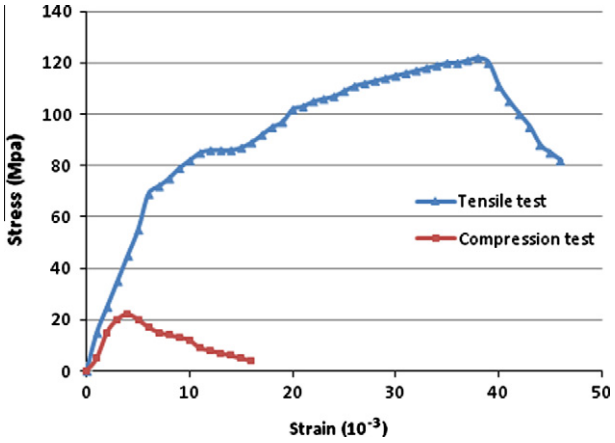


**Fig. 3.** Stress–strain curve for tensile and compression test loading of Kevlar29/Epoxy with Al 6061-T6 laminated plate.

**Table 3**
The total number of specimens with different variables.

| Thickness (4 mm) | No. of Kevlar-29 layers | Sequence of Al plate | Volume fraction ($V_f$) (%) | Initial velocity impact (m/s) | No. of specimens |
|---|---|---|---|---|---|
| 4 | 6 | 1 | 55 | 180, 210, 240 | 3 |
| 4 | 6 | 4 | 55 | 180, 210, 240 | 3 |
| 4 | 6 | 7 | 55 | 180, 210, 240 | 3 |
| 8 | 14 | 1 | 55 | 240, 270, 300 | 3 |
| 8 | 14 | 8 | 55 | 240, 270, 300 | 3 |
| 8 | 14 | 15 | 55 | 240, 270, 300 | 3 |
| 12 | 22 | 1 | 55 | 300, 330, 360, 400, 300 | 4 |
| 12 | 22 | 13 | 55 | 330, 360, 400 | 4 |
| 12 | 22 | 23 | 55 | 300, 330, 360, 400 | 4 |

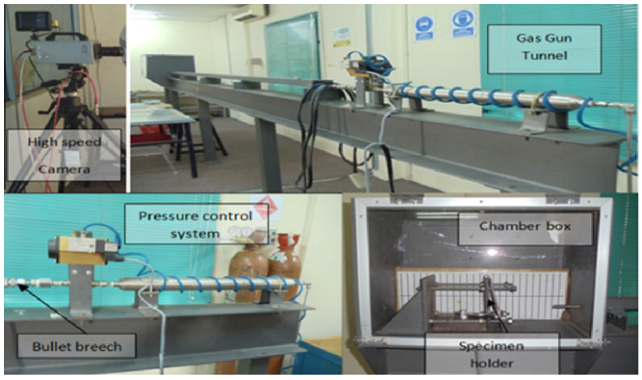


**Fig. 4.** Gas gun tunnel to test the specimens.

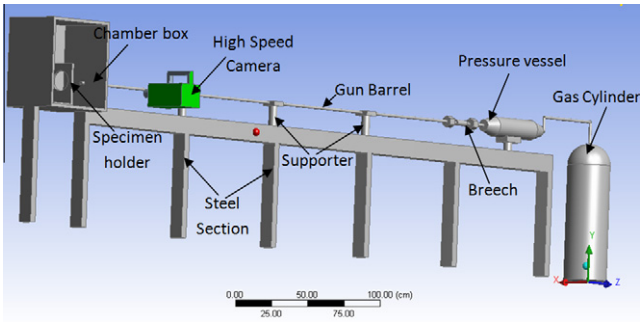


**Fig. 5.** Gas gun tunnel (instrument impact tester).

this box which has a (60 × 60 cm) framing window to observe the behavior of the target and bullet using a high speed camera (200,000 fps) for this work.

The gas gun is capable of launching three types of projectiles (cylindrical, spherical and nose tip) but in this work a cylindrical shape of 7.62 mm diameter steel projectile of weight 5 g 4340 steel bullet (as shown in Fig. 6) was fired to a range of velocity of 180–400 m/s when helium is used as a propellant gas.

In order to set the right pressure for a test, a series of pressure versus velocity shots was carried out and the resulting calibration

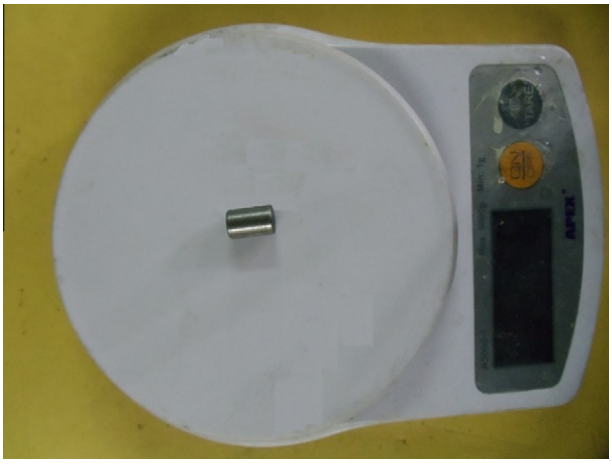

**Fig. 6.** Cylindrical Steel 4340 bullet.

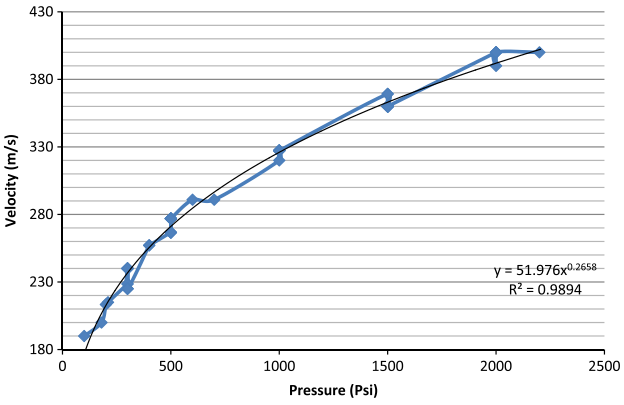


**Fig. 7.** Pressure versus velocity for the gas gun with bore diameter of 8 mm.

curve was used in the various impact tests, shown in Fig. 7. The velocity was always accurately measured with high speed camera.

The projectile is mounted in an 8-piece/serrated sabot with an obturator and inserted into the rear section of the barrel. The target is clamped in a square frame, having an inner and outer clamp of 100 and 200 mm dimensions respectively.

### 2.3. Impact testing

The woven Kevlar-29/epoxy with 6061-T6 Al laminated plates of square shape (100 × 100 mm) with different (4, 8 and 12 mm) thicknesses were placed inside the specimen holder and were focused on by the high speed camera with suitable resolution (200,000 fps) and the ambient light was adjusted to get optimum conditions before each test. Both the alignment of the system and the luminance during testing are crucial parameters in order to have good, reliable images. As indicated above, the high-speed camera system is used for measuring the velocity of projectiles. This is made possible by advanced image processing of the digital pictures while connected to a PC to calculate the time of bullet before impact and after penetration if accrued of specimens as shown in Fig. 8 which shows a 280 m/s velocity impact. The most important feature is the possibility to obtain the initial and residual velocity by the following equations:

$$v_i = \frac{\Delta S_1}{\Delta t_1} \quad (1)$$

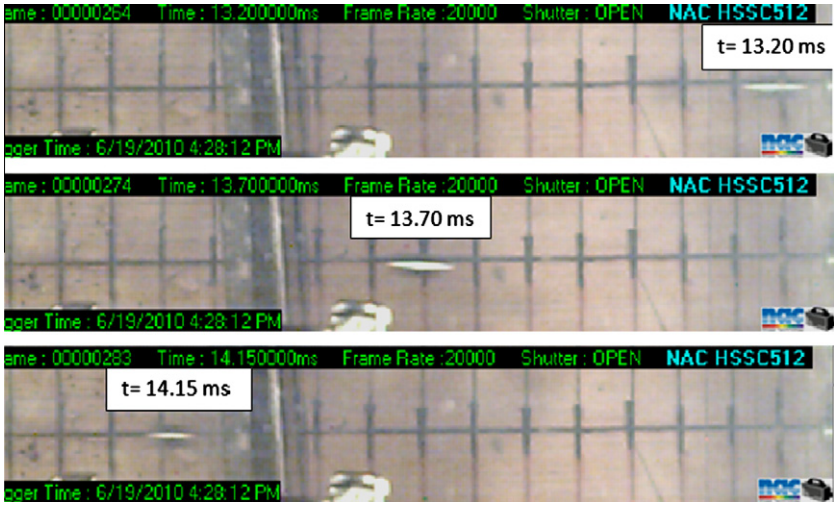


**Fig. 8.** Frames record history by high velocity impact during impact test of specimen.

**Table 4**
Input data used for the analysis, experimental results and predicted results using Autodyn software.

| Property | Ravid et al. [6–8] | | Present experiment (B.S.S) | | | |
|---|---|---|---|---|---|---|
| Rigid projectile | | | | | | |
| Radius (m) | 0.0019 | | 0.00762 | | | |
| Length (m) | 0.0238 | | 13 | | | |
| Density (kg/m$^3$) | 7800 | | 800 | | | |
| Velocities (m/s) | $V_i$ | $V_r$ | $V_{Autodyn}$ | $V_i$ | $V_r$ | $V_{Autodyn}$ |
| | 835[a] | 660[a] | 674[a] | 240[e] | 132[e] | 135[e] |
| | 848[b] | 589[b] | 611[b] | 300[f] | 188[f] | 190[f] |
| | 855[c] | 364[c] | 377[c] | 400[g] | 15[g] | 13[g] |
| | 847[d] | 401[d] | 416[d] | | | |
| Strain coefficient | 0.025 | | | 0.025 | | |
| Target | | | | | | |
| Density (kg/m$^3$) | 7800 | | | 7800 | | |
| Static yield strength (MPa) | 90–120 | | | | | |
| Thickness (m) | 0.06[a] | | | 0.004[e] | | |
| | 0.00635[b] | | | 0.008[f] | | |
| | 0.012[c] | | | 0.012[g] | | |
| | 0.008[d] | | | | | |

[a, b, c, d, e, f, g] Initial, residual velocity (experiment and Autodyn) results based on the thickness of laminate plate.

and

$$V_r = \frac{\Delta S_2}{\Delta t_2} \tag{2}$$

where $V_i$ and $V_r$ initial and residual velocity (m/s) respectively; $S_1$ and $S_2$ displacement before and after penetration (m) respectively and $t_1$, $t_2$ time before and after penetration (s) respectively.

The total energy absorption by the specimen according to the following equation:

$$E_{Abs} = \frac{1}{2} m_p (V_i^2 - V_r^2) \text{ or } E_{Abs} = \frac{1}{2} m_p V_b^2 \tag{3}$$

$$V_b = \sqrt{V_i^2 - V_r^2}$$

where $E_{Abs}$ = energy absorption by the specimen (J); $m_p$ = mass of bullet (kg); $V_b$ = ballistic velocity (m/s).

Ballistic impact performance of the target as used for the experimental studies was also evaluated using the present analytical method. The input data used for the analytical studies is presented in Table 4. For the case of the target with thickness of 4, 8 and12 mm, analytical studies showed that complete perforation of the bullet with exit velocity of back stacking sequence of Al alloy.

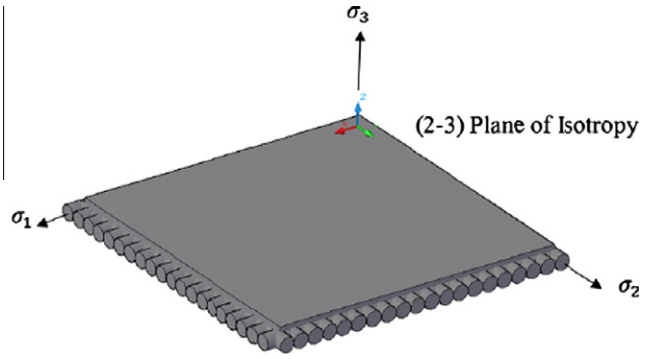


**Fig. 9.** Transverse laminated plates.

## 3. Description of the numerical model

### 3.1. Material modeling

The approach was to first develop material models based on literature research. This was followed by the conduct of proof of concept experiments using suitable materials for each layer which

**Table 5**
Kevlar29/epoxy (orthotropic).

| Temperature (C) | Young's modulus *X* direction (Pa) | Young's modulus *Y* direction (Pa) | Young's modulus *Z* direction (Pa) | Poisson's ratio *XY* | Poisson's ratio *YZ* | Density (kg/m$^3$) |
|---|---|---|---|---|---|---|
| 25° | 1.8e+010 | 1.8e+010 | 1.95e+009 | 8.e−002 | 0.7 | 1230 |

**Table 6**
Al 6061-T6 properties.

| Initial yield stress *Y* (Pa) | Maximum yield stress $Y_{max}$ (Pa) | Shear modulus (Pa) | Hardening exponent *n* | Derivative *dG*/*dP* (G′P) | Derivative *dG*/*dT* *G′T* Pa C$^{-1}$ | Derivative *dY*/*dP* *Y′P* | Melting temperature Tmelt C | Density (kg/m$^3$) |
|---|---|---|---|---|---|---|---|---|
| 2.9e+008 | 6.8e+008 | 2.76e+010 | 0.1 | 1.8 | −1.7e+007 | 1.8908e−002 | 946.85 | 2700 |

**Table 7**
Steel 4340 impactor (Johnson Cook strength).

| Initial yield stress (Pa) | Density (kg/m$^3$) | Bulk modulus (Pa) | Strain rate constant | Thermal softening exponent | Melting temperature C | Reference strain rate (s$^{-1}$) |
|---|---|---|---|---|---|---|
| 7.92e+008 | 7830 | 1.59e+011 | 1.4e−002 | 1.03 | 1519.8 | 1 |

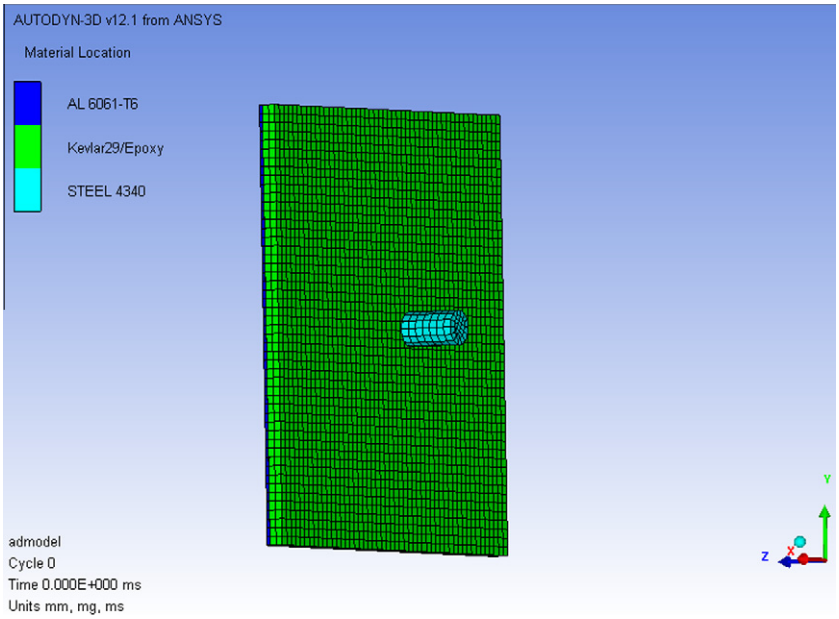


**Fig. 10.** Explicit mesh of 4 mm Kevlar29/epoxy with back Al 6061-T6 plate and Steel 4340 bullet.

satisfy the requirements at each stage to arrest the incoming projectile. The conditions of the experiment (i.e. impact velocity) are then simulated using the numerical model developed so as to make sense of the experimental results. In this paper, the experimental results are presented first, followed by the numerical modeling and simulations.

It is useful to develop a computer model that reproduces the conditions of the experiment so as to allow a comparison with the experimental results. This will also help guide future experiments.

The approach was to use Autodyn software and define the properties of the material used in the experiment based on either literature research or reasonable estimates. Some assumptions are necessary due to the lack of literature values as well as the lack of resources and time to do material testing to obtain the actual mechanical properties. Material models that are used in the simulations are discussed first, and the simulations are presented thereafter.

Kevlar-29/epoxy are unique in their response to impact loading. To capture the response of such brittle and sophisticated damage mechanisms, Autodyn® uses the Johnsone–Holmquist (JH2) Constitutive Model [31] which captures the progressive damage of composite materials subjected to impact loading.

To elucidate the mechanisms of penetration and the effect of the tile edges on the penetrating projectile for the sSiC case we have conducted a series of computations. All computations were

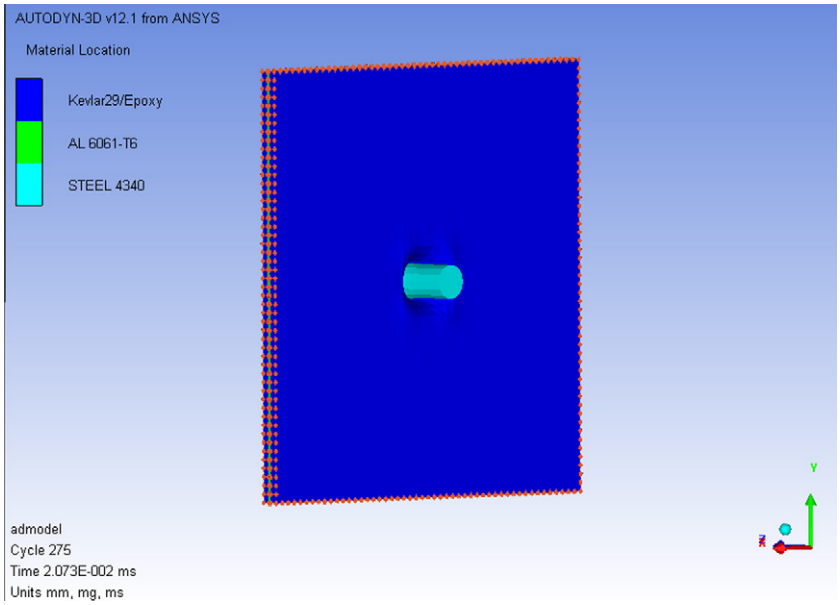


**Fig. 11.** Shows the fixed end of 4 mm of Kevlar29/epoxy with middle stacking sequence Al 6061-T6 plate subjected to 240 m/s Steel 4340 bullet.

carried out using 2D axial symmetry using a Lagrangian mesh in the explicit non-linear transient dynamic numerical code Autodyn-2D. This software is explained in detail elsewhere [32] and a useful overview of these types of codes is provided by Hazell et al. [18]. However in brief, this code solves the conservations laws of mass and momentum based on initial boundary conditions. The user is prompted for an equation of state that describes the pressure in terms of the internal energy and volume and a constitutive relationship that calculates the flow stress in terms of a number of material and application-dependent parameters including strain, strain-rate and temperature. Failure models can be introduced to describe the failure.

Generalized Hooke's law now can be written in matrix from (81 elastic constants):

$$\begin{bmatrix}\sigma_{11}\\ \sigma_{22}\\ \sigma_{33}\\ \tau_{23}\\ \tau_{13}\\ \tau_{12}\end{bmatrix} = \begin{bmatrix}C_{11} & C_{12} & C_{13} & C_{14} & C_{15} & C_{16}\\ C_{12} & C_{22} & C_{23} & C_{24} & C_{25} & C_{26}\\ C_{13} & C_{23} & C_{33} & C_{34} & C_{35} & C_{36}\\ C_{14} & C_{24} & C_{34} & C_{44} & C_{45} & C_{46}\\ C_{15} & C_{25} & C_{35} & C_{45} & C_{55} & C_{56}\\ C_{16} & C_{26} & C_{36} & C_{46} & C_{56} & C_{66}\end{bmatrix}\begin{bmatrix}\epsilon_{11}\\ \epsilon_{22}\\ \epsilon_{33}\\ \gamma_{23}\\ \gamma_{13}\\ \gamma_{12}\end{bmatrix} \tag{4}$$

(where $[C_{ij}]$ is the stiffness matrix)

An orthotropic material is called transversely isotropic when one of its principal planes is a plane of isotropy. The mechanical properties at every point on this plane are the same in all directions, the longitudinal Young's modulus that is in a direction parallel to the fibers, $E_{11}$, can be calculated by simple rules of mixtures for continuous filament composites:

$$E_{11} = E_f V_f + E_m V_m \tag{5}$$

The transverse Young's modulus; the perpendicular direction to the fibers, $E_{22}$, was calculated and estimated simple rule of mixtures for continuous filament composites by Whitney [33] and Mutasher [34] as follows:

$$E_{22} = \frac{E_m(1+\zeta\eta V_f)}{(1-\eta V_f)} \tag{6}$$

where

**Table 8**
Connections of contact regions for Kevlar29/epoxy to Al 6061-T6.

| Object name | Bonded – Kevlar29-Epoxy1 To Al 6061-T6 | Bonded – Al 6061-T6 To Kevlar29-Epoxy2 |
|---|---|---|
| State | Fully defined | |
| *Scope* | | |
| Scoping method | Geometry selection | |
| Contact | 1 Face | |
| Target | 1 Face | |
| Contact bodies | Kevlar29-Epoxy1 | Al 6061-T6 |
| Target bodies | Al 6061-T6 | Kevlar29-Epoxy2 |
| *Definition* | | |
| Type | Bonded | |
| Scope mode | Automatic | |
| Behavior | Symmetric | |
| Maximum offset | 1.e−007 m | |
| Breakable | No | |
| Suppressed | No | |

$$\eta = \frac{(E_f/E_m)-1}{(E_f/E_m)+\zeta} \tag{7}$$

and $\zeta$ is an empirical parameter introduced by Barbero [35], and

$$G_{l2} = l/[(V_f/G_f)+(l-V_f)/G_m] \tag{8}$$

where $G_m$ – modulus of rigidity of the matrix

Note that from Eqs. (7), (8) represent a few of the many micromechanical expressions developed to predict the behavior of fiber-reinforced composite materials for three dimension shown in Fig. 9.

$$\begin{Bmatrix}\sigma_1\\ \sigma_2\\ \sigma^3\\ \tau_4\\ \tau_5\\ \tau_6\end{Bmatrix} = \begin{bmatrix}C_{11} & 0 & 0 & 0 & 0 & 0\\ C_{21} & C_{22} & 0 & 0 & 0 & 0\\ C_{12} & C_{23} & C_{22} & 0 & 0 & 0\\ 0 & 0 & 0 & \frac{C_{22}-C_{23}}{2} & 0 & 0\\ 0 & 0 & 0 & 0 & C_{55} & 0\\ 0 & 0 & 0 & 0 & 0 & C_{55}\end{bmatrix}\begin{Bmatrix}\in_1\\ \in_2\\ \in_3\\ \gamma_4\\ \gamma_5\\ \gamma_6\end{Bmatrix} \tag{9}$$

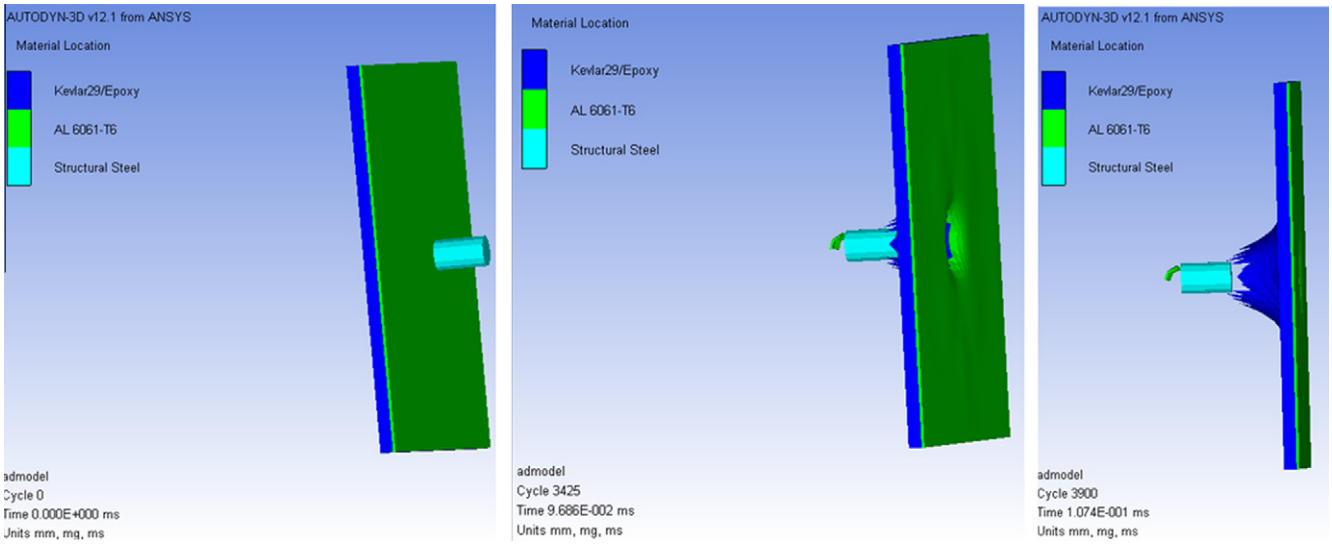


**Fig. 12.** Shows (100 × 100 × 4 mm) Kevlar29/epoxy with front Al 6061-T6 plate subjected to 240 m/s Steel 4340 at different cycles.

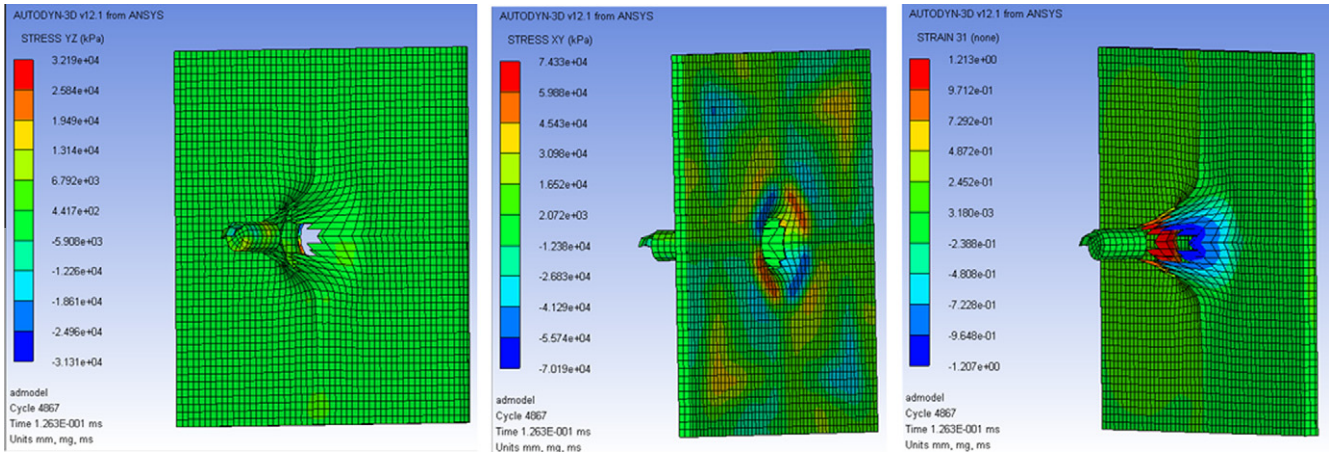


**Fig. 13.** Shows the stress and strain of (100 × 100 × 4 mm) Kevlar29/epoxy with front Al 6061-T6 plate subjected to 240 m/s Steel 4340 at different cycles.

Before the damage initiation, the woven Kevlar-29 fiber laminate is modeled as an orthotropic elastic material that specifies the engineering constants.

$$\begin{Bmatrix} \epsilon_{11} \\ \epsilon_{22} \\ \epsilon_{33} \\ \gamma_{12} \\ \gamma_{13} \\ \gamma_{23} \end{Bmatrix} = \begin{bmatrix} 1/E_1 & -\upsilon_{21}/E_2 & -\upsilon_{31}/E_3 & 0 & 0 & 0 \\ -\upsilon_{12}/E_1 & 1/E_2 & -\upsilon_{32}/E_3 & 0 & 0 & 0 \\ -\upsilon_{13}/E_1 & -\upsilon_{23}/E_2 & -1/E_3 & 0 & 0 & 0 \\ 0 & 0 & 0 & 1/G_{12} & 0 & 0 \\ 0 & 0 & 0 & 0 & 1/G_{13} & 0 \\ 0 & 0 & 0 & 0 & 0 & 1/G_{23} \end{bmatrix} \begin{Bmatrix} \sigma_{11} \\ \sigma_{22} \\ \sigma_{33} \\ \gamma_{12} \\ \gamma_{13} \\ \gamma_{23} \end{Bmatrix} \tag{10}$$

When the material is stressed in the $i$-direction, $\upsilon_{ij}$ characterizes the transverse strain in the $j$-direction. In general, both $\upsilon_{ij}$ and $\upsilon_{ji}$ are related with $\upsilon_{ij}/E_i = \upsilon_{ji}/E_j$. Where in this research work, the values for the Kevlar-29 fiber laminates are of three modules $E_1$, $E_2$, $E_3$; Poisson's ratios $\upsilon_{12}$, $\upsilon_{13}$, $\upsilon_{23}$; and the shear modules $G_{12}$, $G_{13}$, and $G_{23}$. The density of the Kevlar-29 fiber is taken as $\rho = 1440\ \mathrm{kg/m^3}$. That the Kevlar fiber laminate layer is produced by placing fiber in a 0°/90° pattern, the material behavior within the laminate plane is similar. In addition there is no need to separate the fiber and resin. Therefore, longitudinal and transverse strengths in tension and compression are taken as the same figures respectively, so do shear strengths. However, the damage initiation which refers to the onset of degradation at a material point is modeled on the base of Hashin's failure criteria. These criteria employ four damage initiation mechanisms, i.e. fiber tension, fiber compression, matrix tension and matrix compression. Taking $\sigma_{11}$, $\sigma_{22}$ and $\sigma_{12}$ as longitudinal, transverse and shear effective stress tensor components within the glass fiber lamina plane, the initial criteria can be expressed as fiber tension.

In this research a load is applied on an FML specimen, fibers and metal are loaded. For an untracked prismatic specimen, or for a cracked specimen far away from the crack tip the stresses in the individual layers can be calculated using Hooke's law and the law of mixtures. When $E$ is the elastic modulus of the hybrid then

$$E_{Tot} = \frac{E_{Al} \cdot t_{Al} + E_{Ar} \cdot t_{Ar}}{t_{Al} + t_{Ar}} \tag{11}$$

$$\sigma_{Tot} = E_{Tot} \cdot \epsilon = \frac{F}{A_{Tot}} \tag{12}$$

The strain $E$ is the same for every layer in the laminate. The stresses in the individual layers are

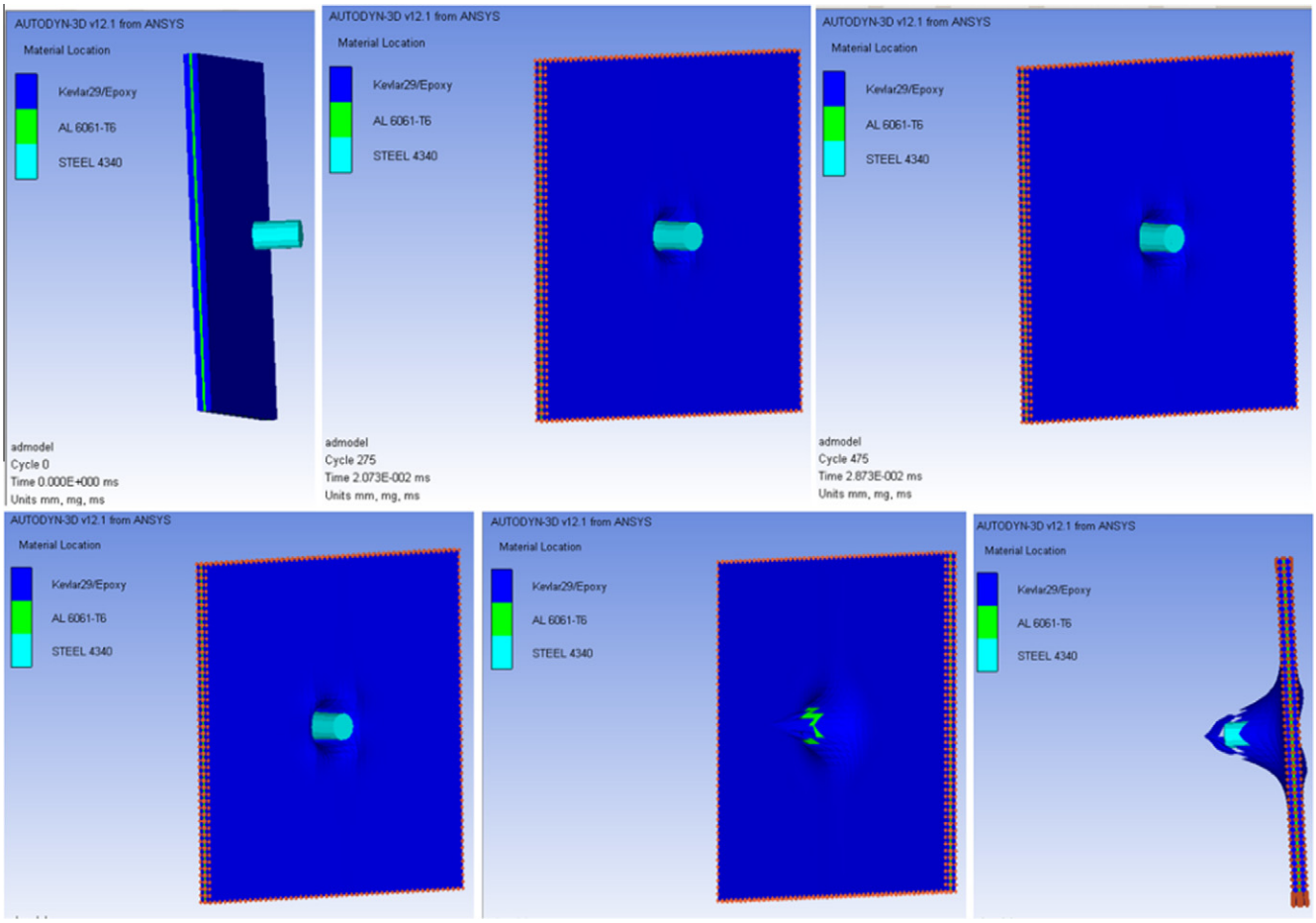


**Fig. 14.** Shows (100 × 100 × 4 mm) Kevlar29/epoxy with middle Al 6061-T6 plate subjected to 240 m/s Steel 4340 at different cycles.

$$\sigma_{Al} = \frac{F}{A_{Tot}} * \frac{E_{Al}}{E_{Tot}} \tag{13}$$

$$\sigma_{Ar} = \frac{F}{A_{Tot}} * \frac{E_{Ar}}{E_{Tot}} \tag{14}$$

where the symbol $t$ means the total materials thickness in the laminate (sum of the thickness of the individual layers' of one material). $E$ is Young's modulus. $F$ is the external load. $A$ is the cross section area and the indices Al, Ar and tot refer to the aluminum, the aramid and the total hybrid, respectively. The residual stresses in a laminate as they occur after curing were calculated from the curvature of an asymmetric laminate after curing. The main properties of fiber Kevlar29/epoxy resin, Al 6061-T6 and Steel 4340 were used in this simulation shown in Table 5–7.

The Johnson–Cook failure model has been used for projectile material, deformations were observed in the cylindrical Steel 4340 bullet as shown in Table 7.

### 3.2. Finite element mesh and Autodyn simulation

The finite element model by Lagrange model using ANSYS v12.1 is shown in Fig. 10, where a sandwich plate is idealized using the same condition in experimental work like fixed end of plate as shown in Fig. 11, thickness of plates, stacking sequences of Al plate mechanical properties, initial velocity of bullet and the properties of bullet. Explicit mesh element was used to simulate the target and the impactor by Academic Autodyn 3D version 12.1. Each layer of the plate was modeled using two solid elements through the thickness, and the minimal element size was 0.2 × 0.2 mm at the plate, which was the point of impact.

The contact regions between Al 6061-T6 and Kevlar29/epoxy was used as a bonded type for this Autodyn simulation as shown in Table 8

## 4. Results and discussion

The predicted damages by Autodyn-3D v12.1 software of the perforation of the 100 × 100 × 4 mm targets as listed in Table 3 with different Al 6061-T6 plate stacking sequences by a 240 m/s strike velocity of Steel 4340 bullet are shown in Figs. 12–16 at different cycles.

The simulation was done using the same conditions as in the experimental work so as to obtain a good comparison.

The Autodyn software has many options to alter the appearance of the results and boundary conditions as shown is Fig. 15, which shows the mesh of the laminated plate, and its stress and strain distribution which results from the damage that occured in the specimen. Fig. 14 shows the boundary conditions of the fixed end of the specimen with a middle Al plate stacking sequence. Fig. 16 shows the stress distribution of the back Al plate stacking sequence. The Figs. 12–16 show the damages of the specimens for the inlet and outlet of the steel bullet and the deformation which occurred in the targets. Front, middle and back Al plate stacking sequences are also shown in these Figures. To compare the damage that occurred during this simulation with experimental test, Fig. 17 shows the specimen after that test of front Al plate stacking sequence and Fig. 18 for back Al stacking sequence, while Fig. 19

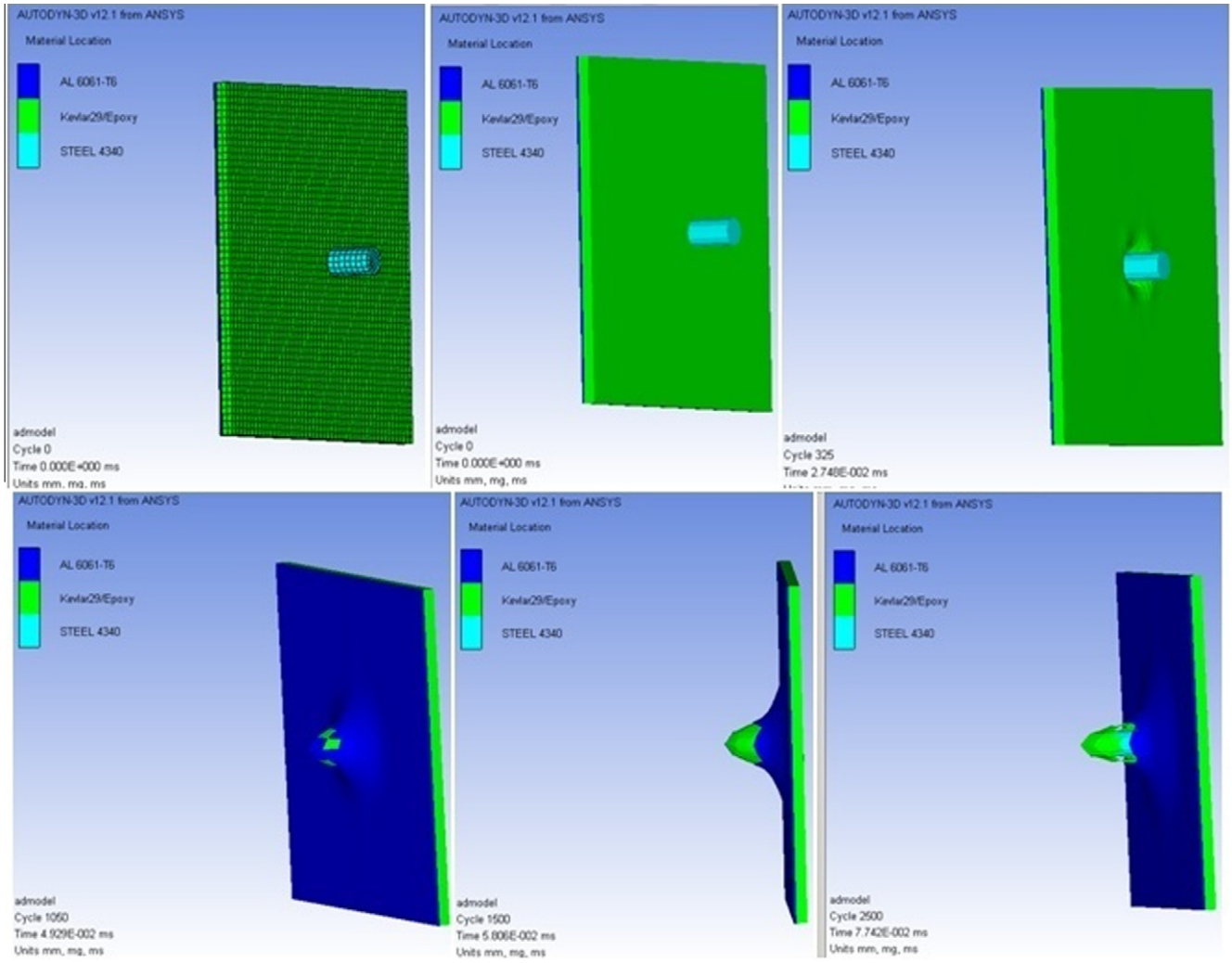


**Fig. 15.** Shows (100 × 100 × 4 mm) Kevlar29/epoxy with back Al 6061-T6 plate subjected to 240 m/s Steel 4340 at different cycles.

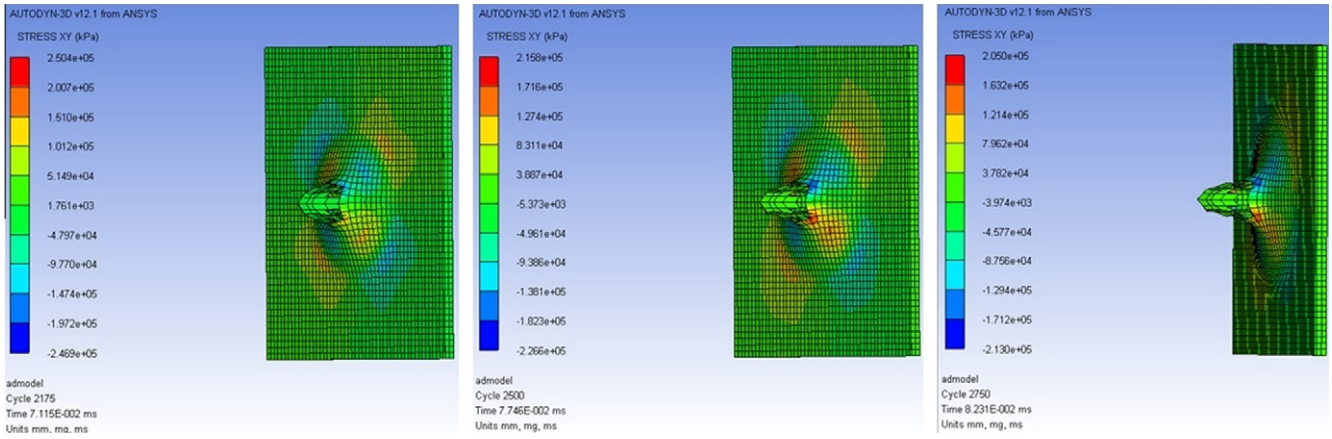


**Fig. 16.** Shows the stress and strain of (100 × 100 × 4 mm) Kevlar29/epoxy with back Al 6061-T6 plate subjected to 240 m/s Steel 4340 at different cycles.

shows the effects on the impactor steel bullet in simulation and experimental test.

The initial velocity versus time of 4 mm laminated plate thickness with different Al plate (front, middle and back stacking sequences) subjected to 240 m/s steel bullet is presented in Fig. 20 which shows decreasing velocity with increasing time until penetration with the residual velocity still stable after penetration occurs.

The different Al stacking sequence of laminated plate effected on the behavior of velocity or residual velocity, so that means its

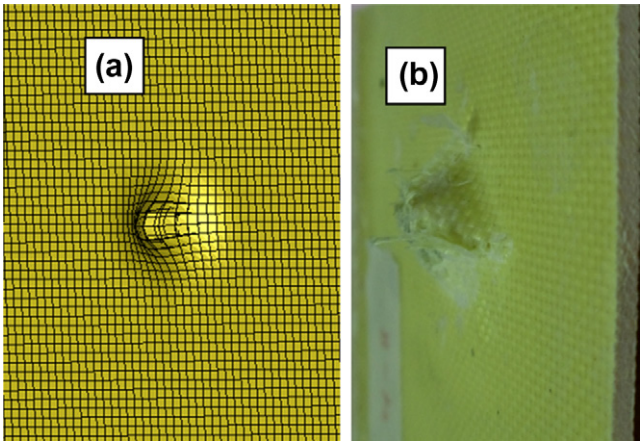


**Fig. 17.** Comparison of the perforated damage in the fabric target in the experimental and theoretical analyses: (a) simulated and (b) observed.

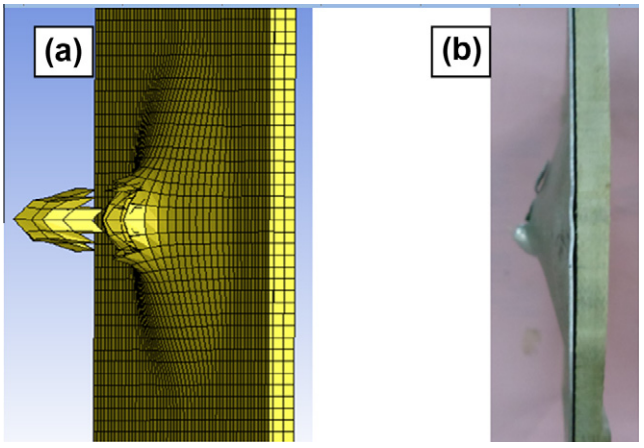


**Fig. 18.** Comparison of the perforated damage in the fabric target in the experimental and theoretical analyses: (a) simulated and (b) observed.

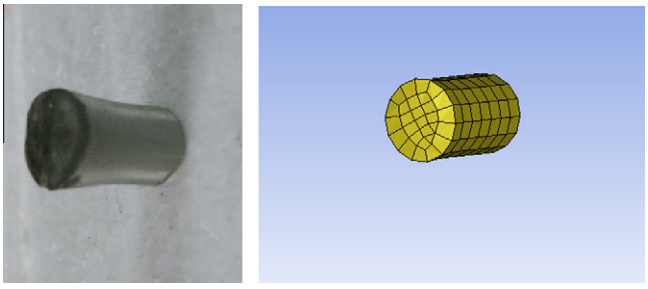

**Fig. 19.** Shows the damage occurred of Steel 4340 bullet at 400 m/s velocity on 12 mm thickness of target.

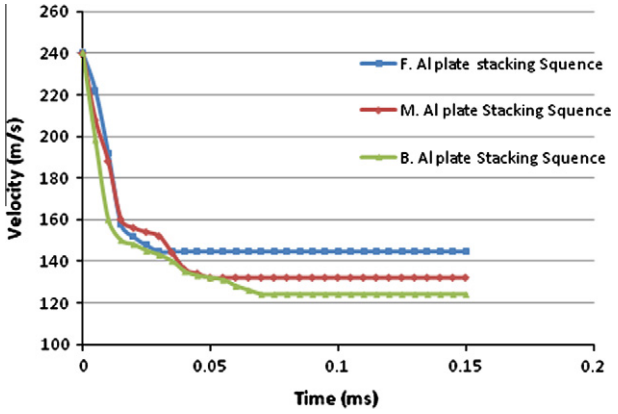


**Fig. 20.** Simulation of time versus velocity of 4 mm target (front, middle and back stacking sequence Al plate) plate subjected to 240 m/s steel bullet.

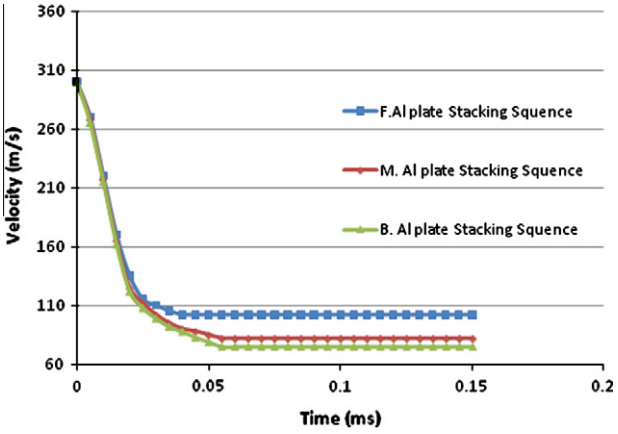


**Fig. 21.** Simulation of time versus velocity of 8 mm target (front, middle and back stacking sequence Al plate) plate subjected to 300 m/s steel bullet.

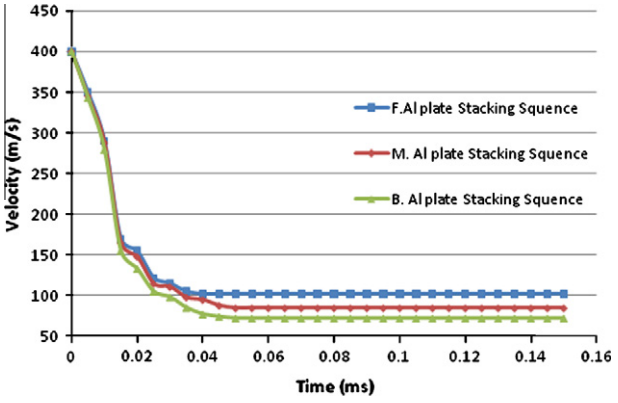


**Fig. 22.** Time versus velocity of 12 mm target (front, middle and back stacking sequence Al plate) plate subjected to 400 m/s steel bullet.

effect on the energy absorption by the specimen according to Eq. (2).

The behavior of time versus residual velocity presented in Figs. 21 and 22 for 8 and 12 mm thickness of laminated plate respectively with different stacking sequence is shown below.

Figs. 23–25 present the residual velocity as a function of the impact velocity for the numerical model simulation and their validation with the experimental results. The numerical simulation by using Autodyn-3D v12.1 obtained a good approximation to the experimental results. The differences between the models and the experimental results are somewhat higher and lower the numerical results.

The energy absorption was also studied in this work to obtain the optimum value and it was found that the maximum relative error of energy absorption between simulation and experimental values is 3.64% for overall results obtained with different thickness, initial velocity and stacking sequence of Al laminated plates as shown in Table 9.

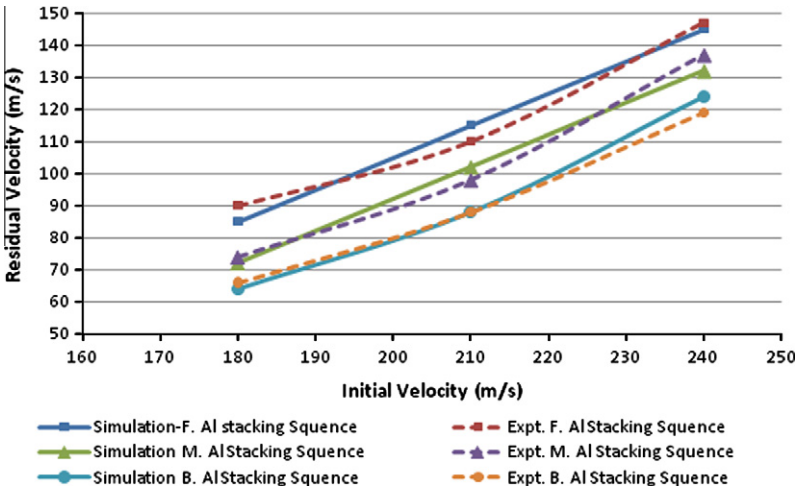


**Fig. 23.** Experimental and simulation results of initial velocity versus residual velocity of (front, middle and back Al plate stacking sequence) 4 mm laminated plate.

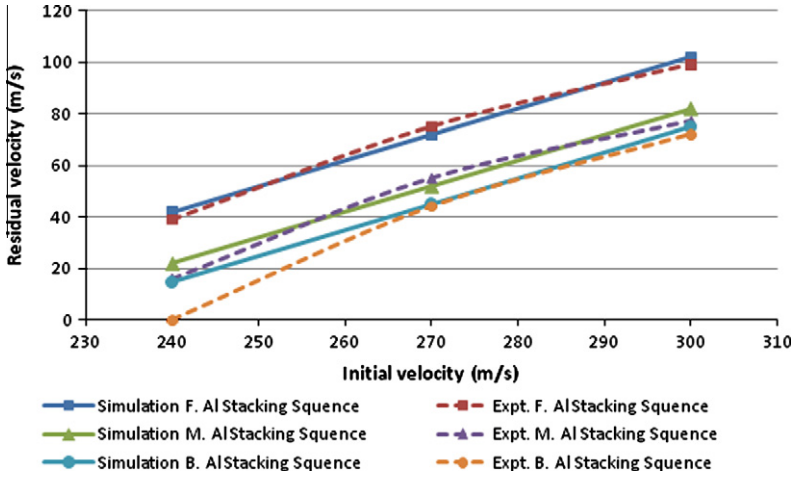


**Fig. 24.** Experimental and simulation results of initial velocity versus residual velocity of (front, middle and back Al plate stacking sequence) 8 mm laminated plate.

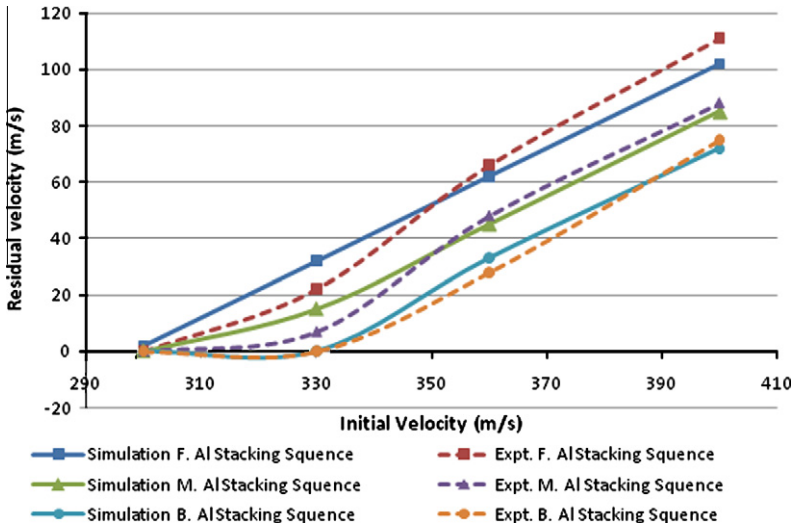


**Fig. 25.** Experimental and simulation results of initial velocity versus residual velocity of (front, middle and back Al plate stacking sequence) 12 mm laminated plate.

From the above table it is clear to see the effect of the stacking sequence on the behavior of energy absorption by targets and normally the increase in thickness of laminated plates leads to the increase of the energy absorption with different velocity.

**Table 9**
Experimental and simulation results of energy absorption of (F – front, M – middle and B – back Al plate stacking sequence) of 4, 8 and 12 mm thickness of laminated plate at different initial velocity.

| Thick (mm) | $V_i$ (m/s) | E. absorp. simulation FSS (J) | E. absorp. experimental FSS (J) | E. absorp. simulation MSS (J) | E. absorp. experimental MSS (J) | E. absorp. simulation BSS (J) | E. absorp. experimental BSS (J) |
|---|---|---|---|---|---|---|---|
| 4 | 180 | 62.93 | 60.75 | 68.04 | 67.31 | 70.76 | 70.11 |
| | 210 | 77.18 | 80.00 | 84.24 | 86.24 | 90.89 | 90.89 |
| | 240 | 91.43 | 89.97 | 100.44 | 97.07 | 105.56 | 108.59 |
| 8 | 240 | 139.59 | 140.19 | 142.79 | 143.36 | 143.43 | 144.00 |
| | 270 | 169.29 | 168.18 | 175.49 | 174.68 | 177.18 | 177.41 |
| | 300 | 198.99 | 200.49 | 208.19 | 210.17 | 210.93 | 212.04 |
| 12 | 300 | 224.99 | 225.00 | 225.00 | 225.00 | 225.00 | 225.00 |
| | 330 | 269.69 | 271.04 | 271.68 | 272.12 | 272.25 | 272.25 |
| | 360 | 314.39 | 313.11 | 318.93 | 318.24 | 321.27 | 322.04 |
| | 400 | 373.99 | 369.19 | 381.93 | 380.64 | 387.04 | 385.93 |

## 5. Conclusions

As a summary of this work, the following conclusions could be found:

- The energy absorption of the composites were increased as the initial velocity increases as shown in Table 8 and the numerical simulation was developed and combined with academic 3D-Autodyn v.12.1 software by explicit mesh to calculate time versus velocity curves and energy absorption of Al 6061-T6 stacking sequence inside the Kevlar29/epoxy composite plates. The impact energy absorptions of numerical simulation compared with experimental work which was calculated by using Eq (3) showed good agreement with maximum error of 3.64%.
- The influence of the Al 6061-T6 stacking sequence inside the laminate of Kevlar29/epoxy composite plates on the behavior of energy absorption by the specimens and ballistic limit for the projectile as shown in Table 8 shows the Al back stacking sequence plate (No. 7, 15 and 23 shown in Table 3) for overall results obtained was the optimum structure to resist the impact loading.
- The simulation model developed predicted with accuracy the residual velocity of steel cylinder projectiles when penetrating Kevlar29/epoxy woven with Al laminated plates. The model considers three different thicknesses of these laminated plates. It used a Lagrange model of Autodyn v.12.1 to optimize the stacking sequence of composite laminates in order to minimize the backplane displacement when subjected to a high velocity impact and used an explicit finite element package.

## Acknowledgments

The authors would like to show their appreciation to University Putra Malaysia for supporting the research activity. Special thanks to Mr. E. Gires for proof read the paper.

## References

[1] Hazell PJ, Appleby-Thomas GJ, Kister G. Impact, penetration, and perforation of a bonded carbon–fibre-reinforced plastic composite panel by a high-velocity steel sphere: an experimental study. Analysis 2010;45:439–50.
[2] Zhu G, Goldsmith W, Dharan CKH. Penetration of laminated Kevlar by projectiles I. Experimental investigation. Int J Solids Struct 1992;29:399–420.
[3] Hou W, Zhu F, Lu G, Fang D-N. Ballistic impact experiments of metallic sandwich panels with aluminium foam core. Int J Impact Eng 2010;37:1045–55.
[4] Cheng WL, Langlie S, Itoh S. High velocity impact of thick composites. Int J Impact Eng 2003;29:167–84.
[5] Zhao G, Cho C, Lu S, Wang Z. Experimental study on impact resistance properties of T300/epoxy composite laminates. J Compos Mater 2009;44:857–70.
[6] Ravid M, Bodner SR, Holcman I. Penetration into thick targets – refinement of a 2D dynamic plasticity approach. Int J Impact Eng 1994;15(4):491–9.
[7] Ravid M, Bodner SR, Holcman I. A two dimensional analysis of penetration by eroding projectiles. Int J Impact Eng 1994;15(5):587–603.
[8] Ravid M, Bodner SR. Dynamic perforation of viscoplastic plates by rigid projectiles. Int J Eng Sci 1983;21(6):577–91.
[9] Silva M. Numerical simulation of ballistic impact on composite laminates. Int J Impact Eng 2005;31:289–306.
[10] Hazell P, Thomas G. A study on the energy dissipation of several different CFRP-based targets completely penetrated by a high velocity projectile. Compos Struct 2009;91:103–9.
[11] Tan V, Khoo K. Perforation of flexible laminates by projectiles of different geometry. Int J Impact Eng 2005;31:793–810.
[12] Kumar S, Singh I, Sharma A. Behavior of Kevlar/epoxy composite plates under ballistic impact. J Reinf Plast Compos 2009;29:2048–64.
[13] Naik N, Doshi A. Ballistic impact behaviour of thick composites: parametric studies. Compos Struct 2008;82:447–64.
[14] Nemat-Nasser S, Sarve S, Isaacs JB, Lischer DW. Novel ideas in multi-functional ceramic armor design. Ceram Trans 2002;134:511–25.
[15] Grujicic M, Pandurangan B, Zecevici U, Koudela KL, Cheeseman BA. Ballistic performance of alumina/S-2 glass-reinforced polymer–matrix composite hybrid lightweight armor against armor piercing (AP) and non-AP projectiles multidiscip model. Mater Struct 2007;3(3):287–312.
[16] Johnson GR, Holmquist TJ. An improved computational constitutive model for brittle materials. New York: High pressure science and technology AIP; 1994.
[17] Clegg RA, Hayhurst CJ, Leahy JG, Deutekon M. Application of a coupled anisotropic material model to high velocity impact response of composite textile armor. In: 18th International symposium on ballistics, San Antonio, TX; 1999.
[18] Hazell PaulJ, Roberson ColinJ, Moutinho Mauricio. The design of mosaic armour: The influence of tile size on ballistic performance. Mater Des 2008;29:1497–503.
[19] Zhang XF, Li YC. On the comparison of the ballistic performance of 10% zirconia toughened alumina and 95% alumina ceramic target. Mater Des 2010;31:1945–52.
[20] Ubeyli M, Deniz H, Demir T, Ogel B, Gurel B, Kele O. Ballistic impact performance of an armor material consisting of alumina and dual phase steel layers. Mater Des 2011;32:1565–70.
[21] Reyes G, Rangaraj S. Fracture properties of high performance carbon foam sandwich structures, composites Part A. Appl Sci Manuf 2011;42:1–7.
[22] Villanueva R, Cantwell WJ. The fracture properties of lightweight fiber-reinforced aluminum foam sandwich structures. In: Proceedings of ASC-16th technical conference, Blacksburg, Blacksburg, VA, USA; 2001 [Paper No. 062].
[23] Villanueva R, Cantwell WJ. Low velocity impact response of novel fiber-reinforced aluminum foam sandwich structure. J Mater Sci Lett 2003;22:417–22.
[24] Villanueva R, Cantwell WJ. Failure mechanisms in composite reinforced aluminum foam sandwich structures. In: Proceedings of the SAMPE symposium and exhibition, Long Beach, CA, USA; 2004.
[25] Reyes G. Mechanical behavior of thermoplastic FML-reinforced sandwich panels using an aluminum foam core: experiments and modeling, experiments and modeling. J Sandwich Struct Mater 2010;12:1099–6362.
[26] Gower HL, Cronin DS, Plumtree A. Ballistic impact response of laminated composite panels. Int J Impact Eng 2008;35:1000–8.
[27] Loikkanen M, Powell D. Simulation of ballistic impact on composite panels. Mech Eng 2008:1–12.
[28] Wijk AG. High-velocity projectile penetration into thick armour targets. Int J Impact Eng 1999;22:45–54.
[29] Weinberg A, Schwartz P. Effect of fibre volume fraction on the strength of Kevlar-29/epoxy strands. J Mater Sci Lett 1987;6:183–4.
[30] Sultan MTH. High velocity impact analysis of glass-epoxy laminated plates. Malaysia: UPM University; 2007.
[31] Holmquist TJ, Johnson GR. Response of boron carbide subjected to high velocity impact. Int J Impact Eng 2008;35:742e52.

[32] Robertson N, Hayhurst C, Fairlie G. Numerical simulation of impact and fast transient phenomena using AUTODYNTM-2D and 3D. Nucl Eng Des 1994;150:235–41.
[33] Whitney JM. Elastic moduli of unidirectional composite with anisotropic filament. J Compos Mater 1968;1:188–93.
[34] Mutasher Saad A. Evaluation of mechanical properties of hybrid aluminium/fiber-reinforced composites. Universiti Putra Malaysia; 2006.
[35] Barbero EJ. Introduction to composite materials design. Philadelphia: Taylor & Francis; 1998.